

Steady State Handling

Giorgio Zampieri, Joel Serrao, Gabriel Crivat

Introduction

The model given consisted in a double track model with vehicle parameters and tire coefficients from a formula SAE car. The reference frame convention used is **ISO**.

To produce the wanted *Speed Ramp Test* and *Steer Ramp Test*, the Simulink input blocks were modified in order to achieve the correct speed and steer profiles as desired inputs.

The first test performed was the speed ramp test.

Speed Ramp Test

The desired forward speed profile provided to the controller consisted of a linear ramp starting from 50 km/h, speed kept for the first second, and then growing with slope 0.5 m/s². Regarding the desired steering angle, it was kept constant with a value of 10°.

From the output of the simulation is possible to observe the linear growth of forward speed (1) and a behaviour close to the desired steady state wanted (2).

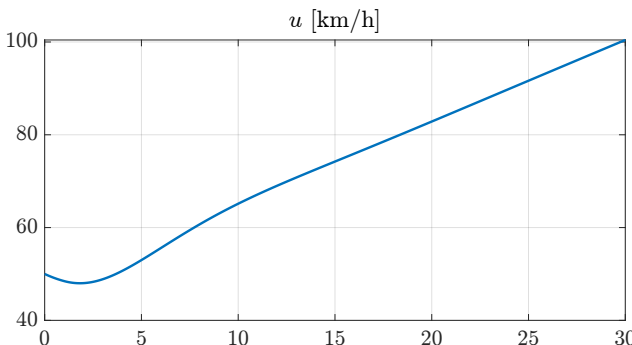


Figure 1: Vehicle Forward Speed

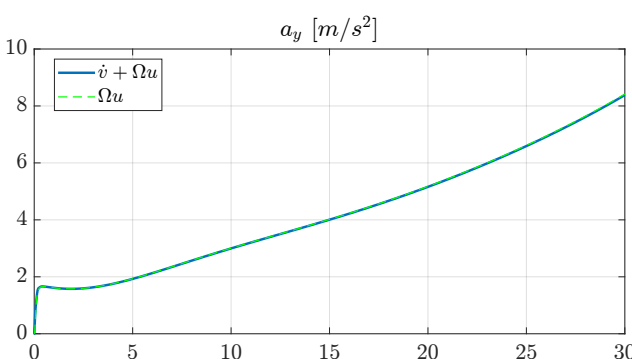


Figure 2: Steady State vs Dynamic Behaviour

Furthermore, the vehicle path shows a collapsing trajectory, i.e. a decreasing radius, highlighting the **oversteering** behaviour of the car (3).

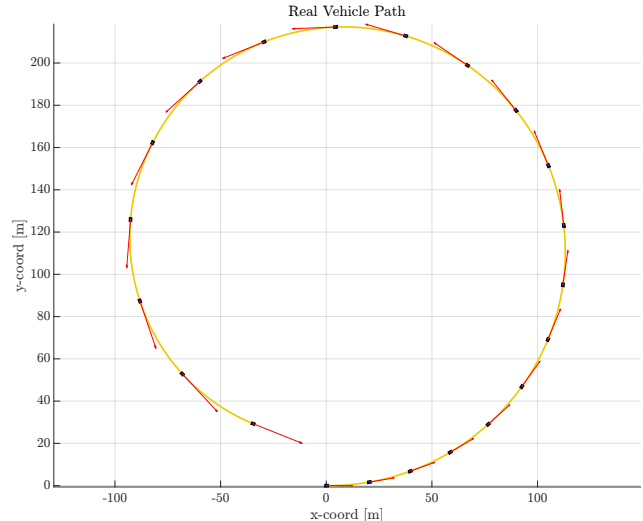


Figure 3: Vehicle Path

Lateral Load Transfer

To estimate the lateral load transfer two approaches were used: the theoretical formula adding elastic and instantaneous contributions:

$$\begin{aligned}\Delta F_{zf} &= ma_y \left(\frac{L_r h_{rf}}{LW_f} + \frac{h_s}{W_f} \epsilon_\phi \right) \\ \Delta F_{zr} &= ma_y \left(\frac{L_f h_{rr}}{LW_r} + \frac{h_s}{W_r} (1 - \epsilon_\phi) \right)\end{aligned}\quad (1)$$

and the average of the normal loads on the tires from the simulation:

$$\begin{aligned}\Delta F_{zf} &= \frac{F_{z,fr} - F_{z,fl}}{2} \\ \Delta F_{zr} &= \frac{F_{z,rr} - F_{z,rl}}{2}\end{aligned}\quad (2)$$

Plotting them together in time (4) and the nominal ones in lateral acceleration (5):

For a positive turn we observe the lateral load transfer growing almost linearly with lateral acceleration. The load transfer is bigger on the rear axle as expected, being stiffer than the front axle ($Ks_f = 1.67 \times 10^4$ N/m, $Ks_r = 2.06 \times 10^4$ N/m).

Axle Characteristics

To compute the normalized axle characteristics, at first the axle apparent side slip were obtained averaging the tire side slips on each axle. These results were then

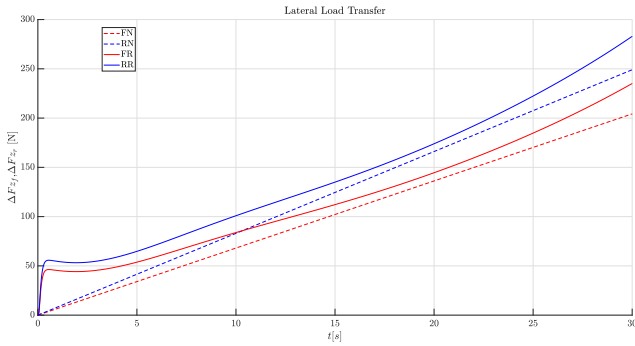
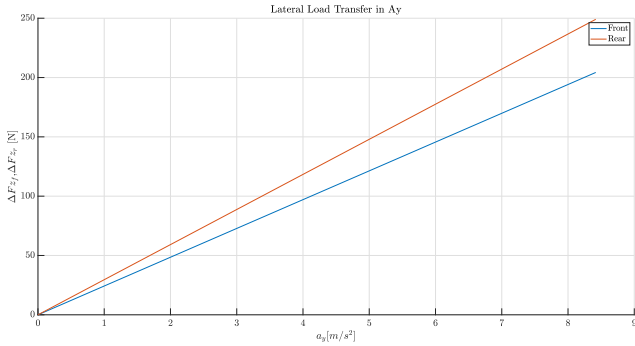


Figure 4: Lateral Load Transfer in time

Figure 5: Lateral Load Transfer in a_y

compared with the ones obtained from the following formulae (**eq.3**) and verified they matched.

$$\begin{aligned}\alpha_f &= \delta_H \tau_H - \beta - \rho_0 L_f \\ \alpha_r &= -\beta + \rho_0 L_r\end{aligned}\quad (3)$$

The axle normal loads F_{z_f}, F_{z_r} were obtained by summing the tires normal loads, averaging out the lateral load transfer. The same method was applied to devise the axle lateral loads F_{y_f}, F_{y_r} . The axle characteristics could have been obtained also by using the following:

$$\begin{aligned}Y_f &= m a_y \frac{L_r}{L} \\ Y_r &= m a_y \frac{L_f}{L}\end{aligned}\quad (4)$$

Finally, the normalized axle characteristics, i.e. the axle adherence were obtained from **eq.5**:

$$\begin{aligned}\mu_f &= Y_f / F_{z_f} \\ \mu_r &= Y_r / F_{z_r}\end{aligned}\quad (5)$$

In figure (12) we can see the lateral loads on each tire for the axles, and the total lateral load. In figure (6) the normalized axle characteristics are showed.

By computing the gradient of the normalized axle characteristics the normalized cornering stiffness C_{y_f}, C_{y_r} are obtained. All these figures are cropped the origin due to a small instability due to the sudden steer angle imposed.

This solution was preferred for speed rather than a slow raise in the δ value, since it causes only a small disturbance during half a second.

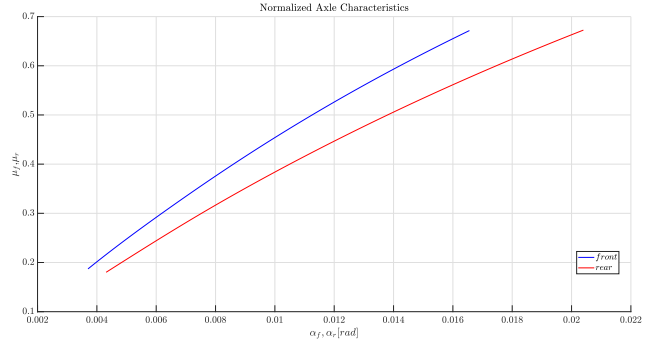


Figure 6: Normalized Axle Characteristics

Handling Diagram

Starting from the steering behaviour of the vehicle:

$$\rho_0 L - \delta_H \tau_H = \alpha_r - \alpha_f \quad (6)$$

The difference $-\Delta\alpha$ was plotted against normalized lateral acceleration. Using the function `polyfit` the tangent to the curve was obtained, and being a first order polynomial fit, the only coefficient is the slope of the steering characteristics, i.e. the understeering gradient K_{US} which is negative with value of -2.84×10^{-4} . Hence, the vehicle shows oversteering behaviour. This fitted value is smaller in modulus w.r.t. the theoretical understeering gradient, this is due to the settling time needed to reach the steady-state conditions. In fact, if the handling characteristic is fitted with a linear polynomial, starting from the moment it presents linear behaviour, thus cutting out the data for low lateral accelerations, then the value of K_{US} is closer to the theoretical value, getting up to -4.07×10^{-4} .

In the lower tiles of (13) the curvature and radius w.r.t. the normalized acceleration of the vehicle are showed, compared with the neutral behaviour. The radius is decreasing for higher lateral accelerations, highlighting an oversteering tendency, matching what was shown in the vehicle position graph.

Yaw Rate Gain

The yaw rate gain $\frac{\Omega}{\delta} = \frac{\rho u}{\delta} = \frac{u}{L(1+K_{US} u^2)}$ is shown in figure (7). The oversteering behaviour of the vehicle is clearly visible: being the steering angle kept constant, the growing curve represents an increase in yaw rate Ω in speed due to growing curvature ρ , i.e. negative understeering gradient.

Body Slip Gain

The body slip gain β/δ is shown in figure (8). The transient phase has strong effects on this result, but, the real simulation output was preferred to represent the body slip gain rather than computing the more

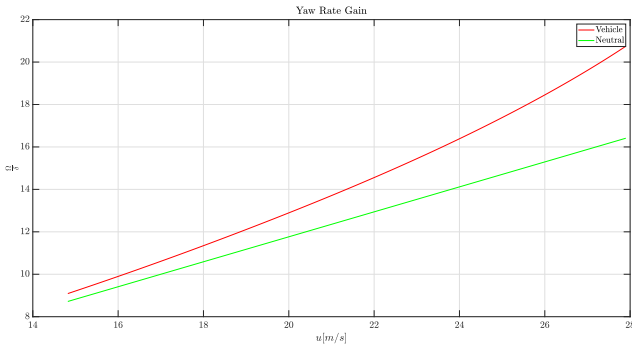


Figure 7: Yaw Rate Gain

fitting theoretical response. To get the neutral curve a simple algebraic simplification was made, imposing $\Delta\alpha = 0$.

$$\begin{aligned} \frac{\beta}{\delta} &= \frac{L_r}{L} - \frac{\alpha_r L_f + \alpha_f L_r}{L\delta} \\ &= \frac{L_r}{L} - \frac{(\Delta\alpha + \alpha_f)L_f + \alpha_f L_r}{L\delta} \\ &= \frac{L_r}{L} - \frac{\alpha_f(L_f + L_r)}{L\delta} \\ &= \frac{L_r}{L} - \frac{\alpha_f}{\delta} \end{aligned} \quad (7)$$

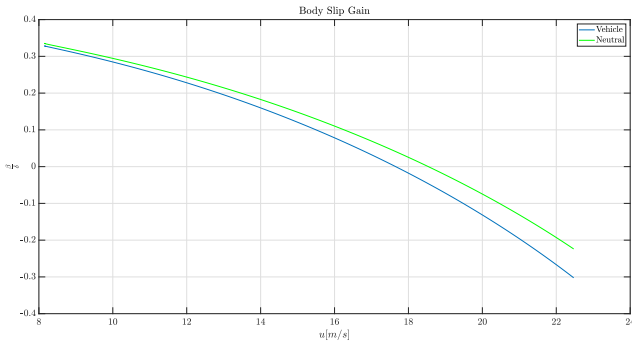


Figure 8: Body Slip Gain

Effects of Parameters

In this final section the speed ramp test was performed varying camber angle, toe steer angle and rolling stiffnesses, in order to observe how the handling diagram would behave.

Camber Effect

The camber angle of the tires was varied from -10° and 10° , while keeping every other vehicle parameter constant. From (9) it is possible to observe that the handling characteristic changes its gradient, getting to a minimum value for angles around 4° and maximum for -10° .

Toe Effect

The toe angle of the tires was varied from -3° and 3° , while keeping every other vehicle parameter constant.

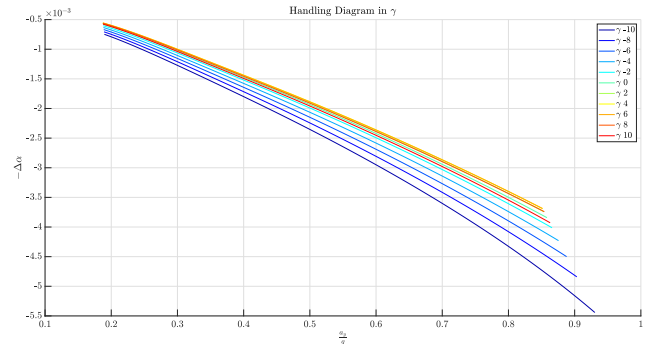


Figure 9: Camber Effect on Handling Diagram

From (10) it is possible to say that a toe angle different from zero causes an increase in the understeering behaviour, especially for negative toe angles.

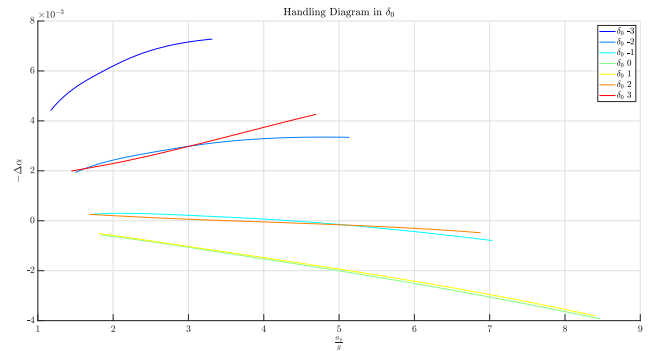


Figure 10: Toe Effect on Handling Diagram

Roll Stiffness Effect

Varying the roll stiffness ratio between front to back the lateral load transfer varies. With respect to the handling diagram, from (11) the effects of ϵ_ϕ are observed. For values close to 0.1, i.e. a stiffer rear axle, the rear slides less, hence it presents under-steering tendencies, reducing the over-steering behaviour. On the other hand, increasing the stiffness in the front axle ($\epsilon_\phi \rightarrow 1$), tends to heighten the over-steering behaviour. Is worth knowing that the vehicle had a stiffness ratio of about $\epsilon_\phi = 0.44$, with behaviour showed in (13).

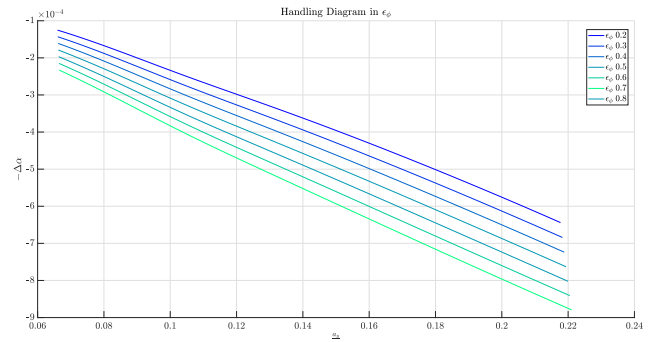


Figure 11: Roll Stiffness Effect on Handling Diagram

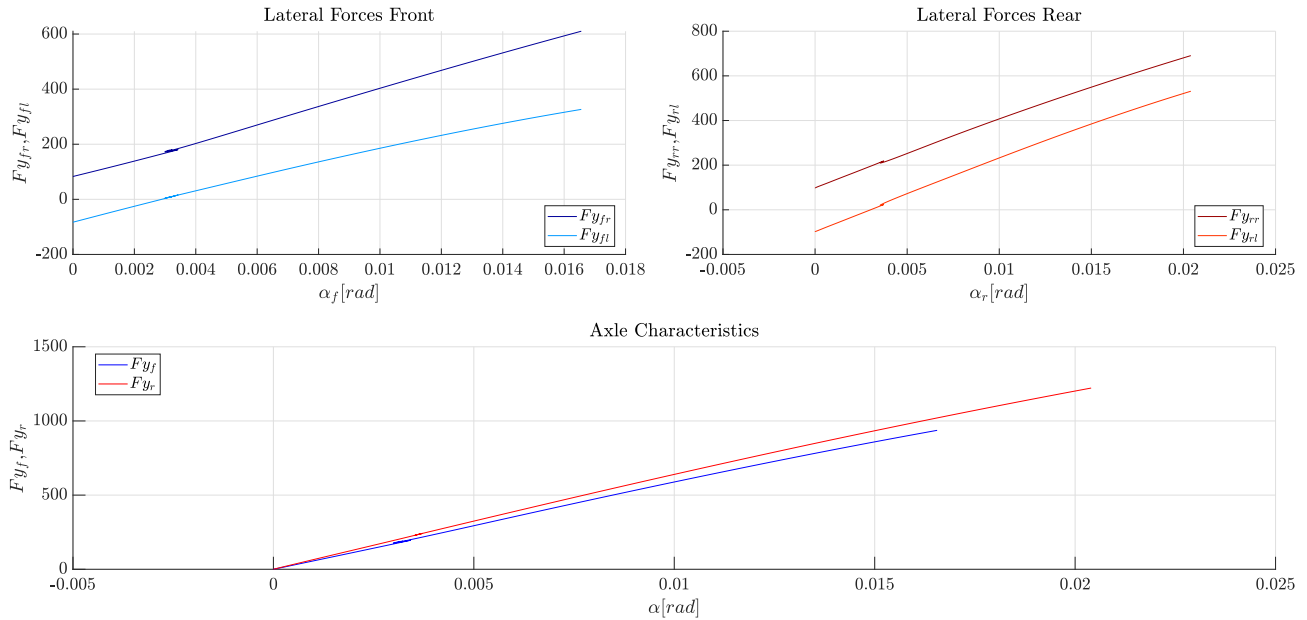


Figure 12: Axe Characteristics

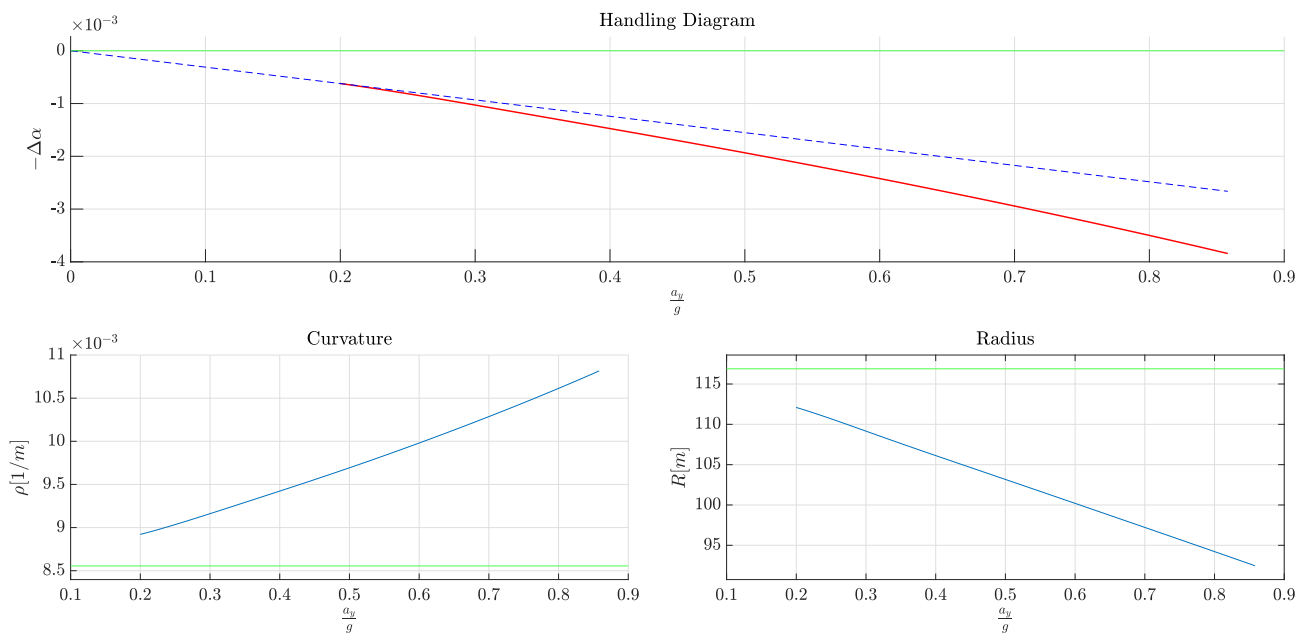


Figure 13: Steering Behaviour

Steer Ramp Test

For the Steering Ramp test, the forward speed is initialized at 0 km/h, and the desired forward speed at the controller is set to 50 km/h. The steering angle is kept at 0° for the first second of the simulation and then starts increasing at a rate of 0.5 °/s².

From the output of the simulation, it can be observed that the vehicle's forward speed is nonlinear for the first twenty seconds before reaching steady-state conditions (14), with the lateral acceleration exhibiting behavior close to the desired steady-state (15).

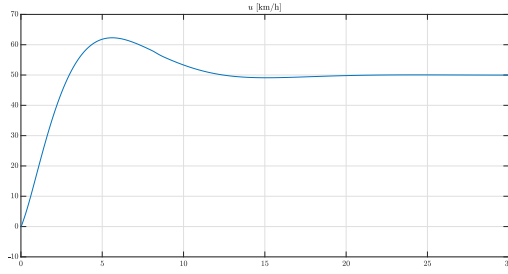


Figure 14: Vehicle Forward Speed

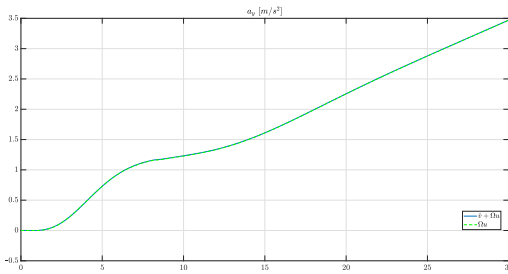


Figure 15: Steady State vs Dynamic Behaviour

Furthermore, in (16) the vehicle's trajectory can be observed.

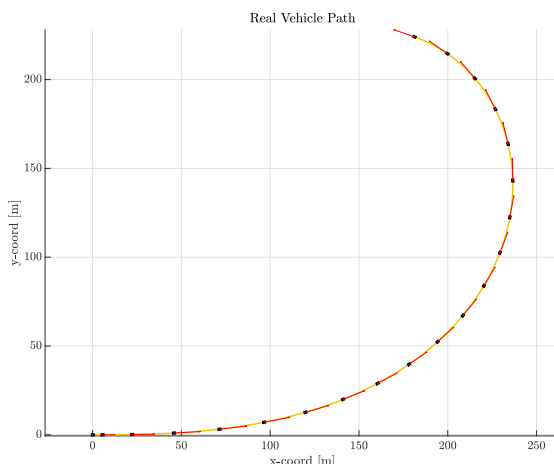


Figure 16: Vehicle Path

Lateral Load Transfer

The theoretical formula, which includes both elastic and instantaneous contributions as shown in eq.1, is compared with the average of the normal loads on the tires obtained from the simulation (eq.2). Both curves are plotted together over time in 17, and the nominal ones are plotted against lateral acceleration in 18.

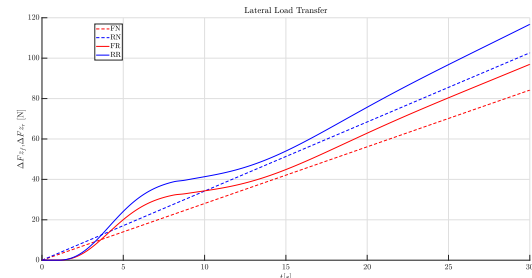


Figure 17: Lateral Load Transfer in time

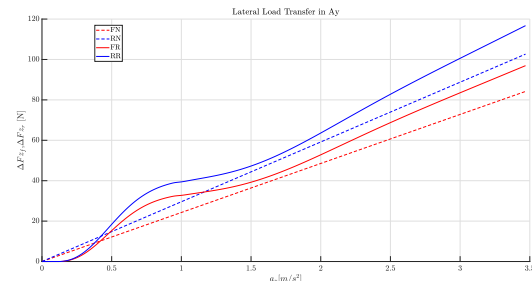


Figure 18: Lateral Load Transfer in a_y

For a positive turn, it is observed that the lateral load transfer grows almost linearly with lateral acceleration. As expected, the load transfer is greater on the rear axle, which is stiffer than the front axle ($K_{sf} = 1.67 \times 10^4$ N/m, $K_{sr} = 2.06 \times 10^4$ N/m).

Axle Characteristics

To compute the normalized axle characteristics, the axle apparent side slip was obtained by averaging the tire side slips on each axle. These results were then compared with the ones obtained from (eq.3) and verified that they matched.

The axle normal loads Fz_f and Fz_r were obtained by summing the tires normal loads and averaging out the lateral load transfer. The same method was applied to derive the axle lateral loads Fy_f and Fy_r .

Finally, the normalized axle characteristics, i.e. the axle adherence, were obtained from eq.5.

In figure (19), the lateral loads on each tire for the axles and the total lateral load are displayed. In Figure (19), the normalized axle characteristics are shown.

By computing the gradient of the normalized axle characteristics, the normalized cornering stiffness Cy_f and Cy_r are obtained.

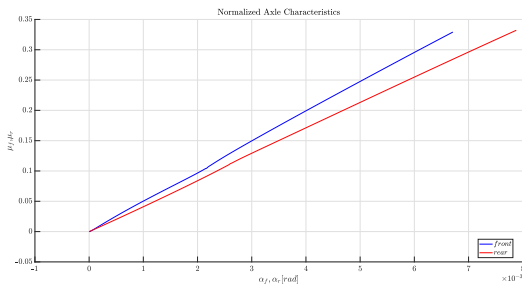


Figure 19: Normalized Axe Characteristics

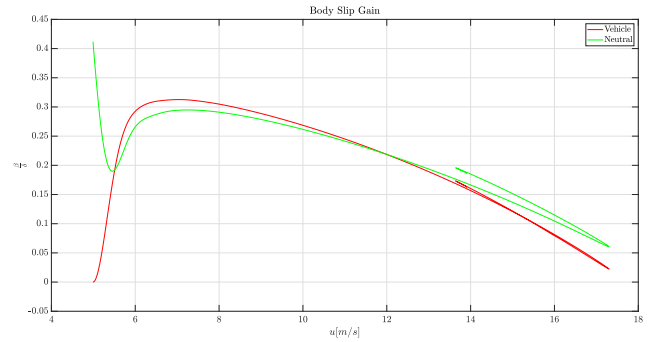


Figure 21: Body Slip Gain

Handling Diagram

The steering behavior of the vehicle is described by (eq.6). The difference $-\Delta\alpha$ was plotted against normalized lateral acceleration, and the tangent to the curve was obtained using the function `polyfit`. Since it is a first-order polynomial fit, the only coefficient represents the slope of the steering characteristics, i.e. K_{US} which is negative with value of -3.43×10^{-4} . Hence, the vehicle shows oversteering behaviour. (the initial understeering tendency is due to transient behaviour)

In the lower tiles of figure (25), the curvature and radius with respect to the normalized acceleration of the vehicle are compared and displayed, along with the neutral behavior. As expected, the radius gradually decreases as the lateral acceleration increases.

Yaw Rate Gain

The yaw rate gain $\frac{\Omega}{\delta} = \frac{\rho u}{L(1+K_{US} u^2)}$ is shown in Figure (20). The growing curve represents an increase in yaw rate Ω with speed due to the growing curvature ρ , indicating a negative understeering gradient.

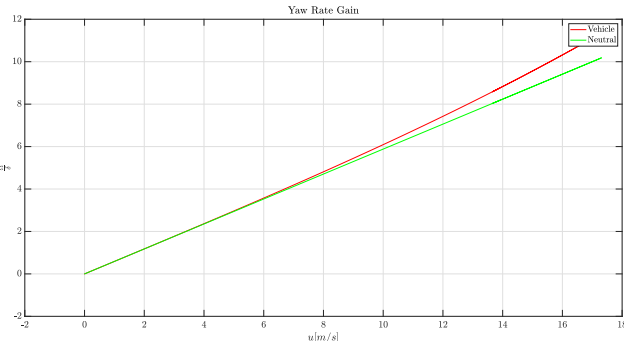


Figure 20: Yaw Rate Gain

Body Slip Gain

The body slip gain β/δ is shown in figure (21). The transient phase has strong effects on this result, but, the real simulation output was preferred to represent the body slip gain rather than computing the more fitting theoretical response. To get the neutral curve a simple algebraic simplification was made, as shown in eq.7.

Effects of Parameters

In this final section, the steer ramp test was performed while varying the camber angle, toe steer angle, and rolling stiffnesses. The objective was to observe how the handling diagram would change under these different conditions.

Camber Effect

The camber angle of the tires was varied from -4° to 4° , while keeping every other vehicle parameter constant. From (22), it is possible to observe that the handling characteristic changes its gradient, always maintaining its general oversteering behavior. However, for positive camber angles, it shows understeering tendencies, while exhibiting more oversteering for negative values. In this test, the angle values were limited due to the onset of instability.

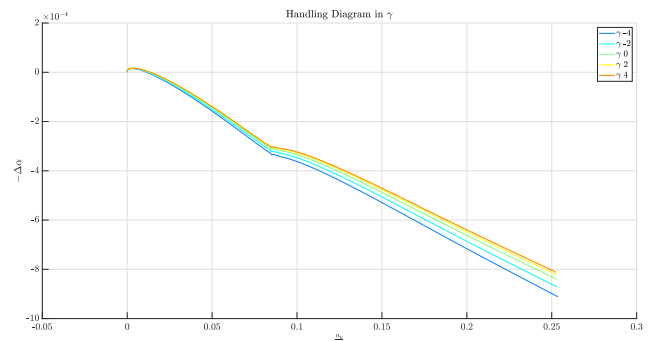


Figure 22: Camber Effect on Handling Diagram

Toe Effect

The toe angle was varied from -3° to 3° for the tires, while all other vehicle parameters were kept constant. From (23), it is evident that toe angle values different from zero lead to an increase in understeering behavior, especially for negative toe angles. Only for 0° and 1° toe angles we observe oversteering behavior.

Roll Stiffness Effect

In the handling diagram from (24), the effects of ϵ_ϕ are observed. For values less than 0.5, i.e. a stiffer

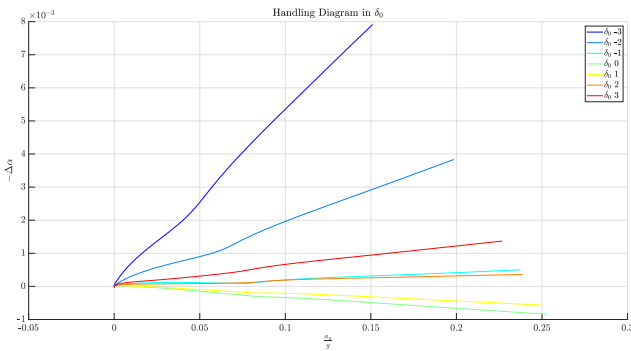


Figure 23: Toe Effect on Handling Diagram

rear axle, the rear slides less, hence it exhibits understeering tendencies, reducing the general oversteering behavior. On the other hand, increasing the stiffness in the front axle ($\epsilon_\phi \rightarrow 1$) tends to heighten the oversteering behavior. It is worth knowing that the vehicle had a stiffness ratio of about $\epsilon_\phi = 0.44$.

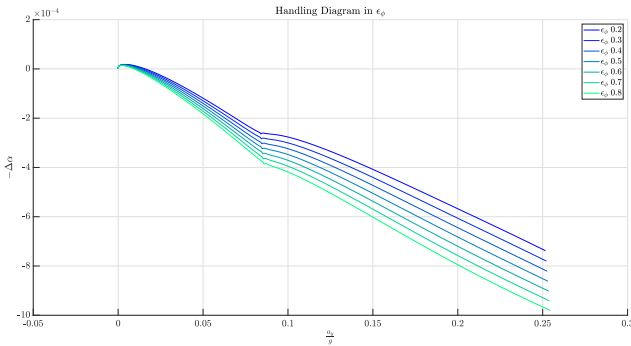


Figure 24: Roll Stiffness Effect on Handling Diagram

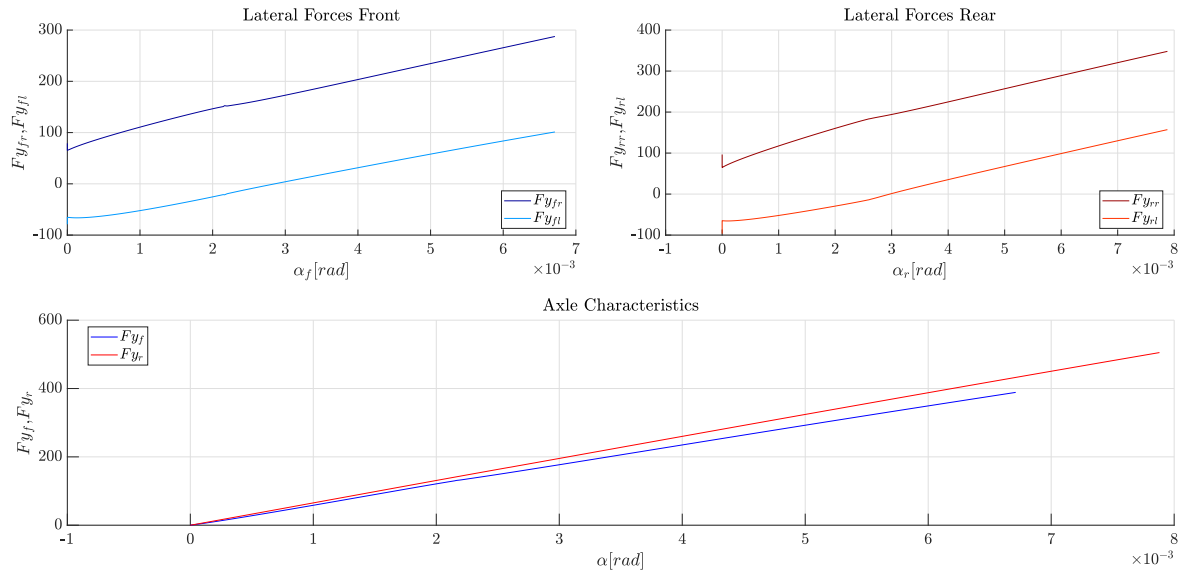


Figure 25: Axe Characteristics

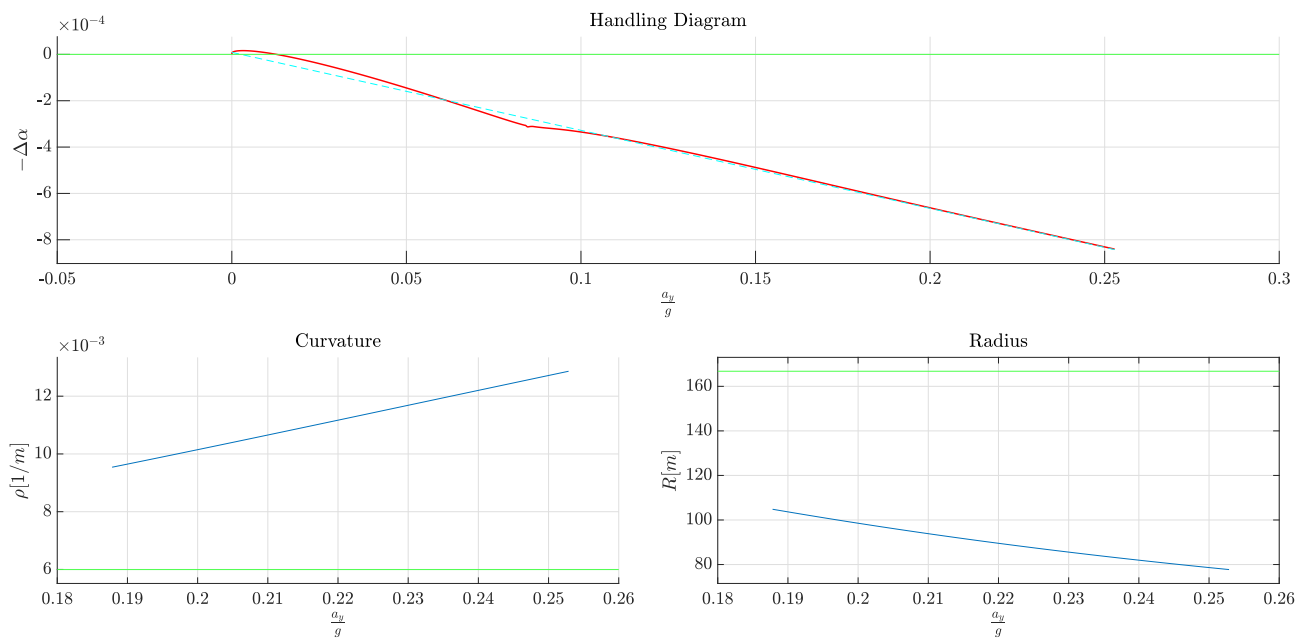


Figure 26: Steering Behaviour